Journal of Electrical Engineering & Technology (2024) 19:1593–1605
https://doi.org/10.1007/s42835-023-01666-x

ORIGINAL ARTICLE

Analysis of Multi-Harmonic Magnetic Field Coupling Characteristics of Bearingless Permanent Magnet Synchronous Motor

Hongbo Qiu[1] · Si Chen[2] · Guangchuan Liang[1] · Cunxiang Yang[2]

Received: 8 June 2023 / Revised: 12 September 2023 / Accepted: 19 September 2023 / Published online: 10 October 2023

Abstract
The suspension performance is an important evaluation index of the bearingless motor, which is the key to avoiding shutdown caused by stator and rotor collisions, as well as the safe and stable operation of the motor. In this paper, an Accurate Decoupling Mathematical Analysis Method for Multi-harmonic Magnetic Field Based on Maxwell Tensor Method. On the basis of the mathematical analysis model of the suspension performance and the analysis of the air gap multi-magnetic field, the weight classification of the influence of coupling magnetic field on radial suspension force is studied. The spatial distribution and temporal variation of the suspension force and its fluctuation are analyzed according to the coupling relationship involving the constant, fluctuating components and the space-time vector in the space-time vector expression of the suspension force, and the relationship between the space–time coupled magnetic field and the suspension performance is obtained. Further combined with numerical analysis, the effect of polar arc eccentricity on suspension performance is analyzed, the optimal eccentricity for suspension performance is found, and the effect of the harmonic magnetic field of permanent magnets on the fluctuation of levitation force is verified. Finally, the prototype is made, the experimental platform was built, and the experimental platform is constructed to test the static and the dynamic performance of the prototype.

Keywords The Maxwell tensor method · Dual windings design · Spatial-temporal multi-harmonic magnetic field coupling · Spatio-temporal vector expressions of suspension force · Suspension force fluctuations

1 Introduction

Bearingless Permanent Magnet Synchronous Motor (BPMSM) is a combination of the magnetic bearing and the permanent magnet synchronous motor, which has the advantages of high efficiency, high speed, low friction loss, long service life, simple structure and reliable operation performance [1–3] and solves the problem of electrical transmission friction under special working conditions. The BPMSM also has an important theoretical and engineering applications in high-tech fields such as centrifuge, turbo molecular pump, flywheel energy storage, high-speed motorized spindle, life science and aerospace [4–6].

Achieving the coincidence between the shaft center and geometric center of the motor is the key factor for the safe and stable operation of BPMSM. During the operation of the BPMSM, the variation of the suspension performance will cause the vibration noise of the motor to increase, and even lead to the collision shutdown failure of the stator and the rotor. In addition, the unilateral magnetic pull during the operation of BPMSM will further affect the suspension stability of the motor and enhance the risk of collision failure. Therefore, the suspension performance directly determines the operational reliability of the BPMSM. At present, scholars have focused on the optimized design of the motor structural for BPMSM, including the novel topology of

✉ Si Chen
chensimail@qq.com

Hongbo Qiu
qiuhongbohrb@163.com

Guangchuan Liang
GuangchuanLiang@outlook.com

Cunxiang Yang
yangzzha@126.com

[1] College of Electrical and Information Engineering, Zhengzhou University of Light Industry, Zhengzhou 450002, Henan, China

[2] College of Building Environmental Engineering, Zhengzhou University of Light Industry, Zhengzhou 450002, Henan, China

motors, the design of stator and rotor, and the optimization of windings.

A novel Halbach rotor permanent magnet synchronous motor structure was proposed in reference [7], which optimized the air gap magnetic field and back electromotive force, and reduced the fluctuations of the radial suspension force and the magnitude of the torque pulsations. A novel segmented dipole interior permanent magnet slice rotor of the bearingless motor was proposed in reference [8], which achieved a reduced tradeoff between force and torque capacity and relatively symmetric force dynamics. In the reference [9], an optimized configuration of the torque winding and suspension winding pole pairs for a rear-pole bearingless motor was investigated to achieve higher torque with larger suspension force. A novel stator main winding structure of a middle-point-current-injection-type bearingless permanent magnet synchronous motor was proposed in reference [10], which did not have additional windings but has only middle-point terminals in the stator motor main windings, the shaft vibration is significantly suppressed, and the system was cost effective. A Novel Axial Split Phase bearingless Flywheel Machine with Hybrid-Inner-Stator Permanent Magnet-Based Structure was proposed in the reference [11], which had complete decoupling of torque and radial suspension force, four degrees-of-freedom (DOF) actively controlled suspension, high torque and radial force density. The reference [12] proposed a design method that used the electromagnetic calculation to determine the structural parameters of the BPMSM, and the high harmonic interference within the motor can be suppressed by using the short pitch winding and the cosine-shape permanent magnet structure. An unequal amplitude modulated magnetic pole structure was proposed in the reference [13], which can effectively reduce the fluctuation of torque and suspension force and improve the performance of bearingless PMSM with the premise of the output capacity.

The above research has optimized the suspension performance of the BPMSM from the aspects of motor structure and winding optimization design. Although the suspension performance of the motor has been further improved, there is a lack of research on the intrinsic factors that cause the variation of the magnitude and fluctuation of the suspension force in the BPMSM, especially the mechanism analysis of the multi-harmonic magnetic field on the magnitude, fluctuation, and direction of the suspension force in the motor.

Based on the mathematical model of the BPMSM, this paper firstly analyzes the characteristics of the air gap magnetic field distribution of the motor and determines the composition of the multi-harmonic magnetic field of the motor. Secondly, combined with Maxwell Tensor Method, the expressions of the multi-harmonic magnetic field and the radial suspension force are obtained. And the influence of the coupling magnetic fields on the magnitude, the fluctuation and the direction of the suspension force is determined, and the distribution of the radial electromagnetic force affected by the coupling magnetic field is given. Meanwhile, combined with the finite element method, the variations of the air gap multi-harmonic magnetic field content caused by the change of the eccentric distance of the permanent magnet are analyzed, and the influence of the magnetic field harmonic content of the permanent magnet on the magnitude and fluctuation of the suspension force is determined. Finally, the variation of the suspension force at different currents and different rotational speeds is obtained, and the test results are also compared with the finite element method and calculation results.

2 The Mathematical Analysis Model of The Suspension Performance of the BPMSM

As a method to analyze the relationship between the multi-harmonic magnetic field parameters and the performance of the motor, the mathematical model can provide an accurate assessment of the suspension performance and improve the efficiency of motor design optimization, meanwhile it also saves a lot of simulation running time. In order to determine the relationship between the magnetic field and the suspension force, the Maxwell Tensor Method is used to decouple the multi-harmonic magnetic field of the motor in this paper.

2.1 The Suspension Force Analysis of the BPMSM

According to the calculation of magnetic tension stresses on the boundary of magnetic substances with different permeability by the Maxwell Tensor Method, the radial electromagnetic force on the rotor surface of BPMSM can be expressed in the unit area, as shown in Eq. 1 [14].

$$\begin{aligned} dF(\theta,t) &= \frac{\mu_{Fe}-\mu_0}{2\mu_{Fe}\mu_0}\left(B_n^2+\mu_{Fe}\mu_0 B_t\right)dS \\ &\xrightarrow[\mu_{Fe}\gg\mu_0]{} = \frac{B^2(\theta,t)dS}{2\mu_0} = \frac{B^2(\theta,t)RldA}{2\mu_0} \end{aligned} \tag{1}$$

The x-axis component of the suspension force and the y-axis component of the suspension force can be expressed as.

$$\begin{cases} dF_x(\theta,t) = dF(\theta,t)\cdot\cos\theta = \dfrac{B^2(\theta,t)Rl\cos\theta d\theta}{2\mu_0} \\ dF_y(\theta,t) = dF(\theta,t)\cdot\sin\theta = \dfrac{B^2(\theta,t)Rl\sin\theta d\theta}{2\mu_0} \end{cases} \tag{2}$$

where, μ_{Fe} and μ_0 are the core and vacuum permeability, respectively; *Bn* and *Bm* are the radial and tangential

magnetic induction intensity at the intersection, respectively; R is the radius of the rotor; l is the core length; and θ is the space angle between any point in the air gap and the x-axis.

2.2 The Analysis of the Magnitude and Direction of the Suspension Force

Under the action of any magnetic fields $b\delta m(\theta,t)$ and $b\delta n(\theta,t)$, the component of the radial suspension force along the x-axis can be expressed as

$$\begin{aligned} F_{xmn} &= \int_0^{2\pi} \frac{Rl}{2\mu_0}\left[b_{\delta m}(\theta,t)+b_{\delta n}(\theta,t)\right]^2\cos\theta d\theta \\ &= \int_0^{2\pi} \frac{Rl}{2\mu_0}\left[B_m\cos\left(P_m\theta-\omega_m t+\varphi_m\right)+\right. \\ &\quad \left. B_n\cos\left(P_n\theta-\omega_n t+\varphi_n\right)\right]^2\cos\theta d\theta \\ &= \frac{RlB_mB_n}{4\mu_0}\int_0^{2\pi}\cos\left[\left(P_m\pm P_n\pm 1\right)\theta-\right. \\ &\quad \left.\left(\omega_m\pm\omega_n\right)t+\left(\varphi_m\pm\varphi_n\right)\right]^2 d\theta \end{aligned} \tag{3}$$

According to the relationship between the angular frequency of the magnetic field and the number of magnetic field poles, the combined suspension force and the components of the suspension force can be further expressed.

$$F_{mag}=\sqrt{\left(F_{xmn}\right)^2+\left(F_{ymn}\right)^2}=\begin{cases}\dfrac{\pi RlB_mB_n}{2\mu_0} & P_m=P_n\pm 1\\ 0 & P_m\neq P_n\pm 1\end{cases} \tag{4}$$

$$F_{xmn}=\begin{cases}\underset{P_m=P_n\pm 1}{\overset{\omega_m\pm\omega_n=0}{\longrightarrow}} \dfrac{\pi RlB_mB_n}{2\mu_0}\cos\left(\varphi_m-\varphi_n\right)\\ \underset{P_m=P_n\pm 1}{\longrightarrow} \dfrac{\pi RlB_mB_n}{2\mu_0}\cos\left[\left(\omega_m-\omega_n\right)t+\left(\varphi_m-\varphi_n\right)\right]\\ \underset{P_m\neq P_n\pm 1}{\longrightarrow} 0\end{cases} \tag{5}$$

$$F_{ymn}=\begin{cases}\underset{P_m=P_n\pm 1}{\overset{\omega_m\pm\omega_n=0}{\longrightarrow}} \dfrac{\pi RlB_mB_n}{2\mu_0}\sin\left(\varphi_m-\varphi_n\right)\\ \underset{P_m=P_n\pm 1}{\longrightarrow} \dfrac{\pi RlB_mB_n}{2\mu_0}\sin\left[\left(\omega_m-\omega_n\right)t+\left(\varphi_m-\varphi_n\right)\right]\\ \underset{P_m\neq P_n\pm 1}{\longrightarrow} 0\end{cases} \tag{6}$$

From (4), (5) and (6), it can be seen that the magnetic field magnitude (B_m and B_n) determines the magnitude of the suspension force, the magnetic field phase (ω_m and ω_n) and the magnetic field angular frequency (φ_m and φ_n) affect the direction of the suspension force. On this basis, the vector relationship diagrams of the magnetic field and the suspension force at different moments of the motor are given in Fig. 1, including the influence of the magnetic field magnitude, the magnetic field phase and the magnetic field angular frequency on the suspension force.

When the magnetic field angular frequency satisfies $\omega_m=\omega_n$, the magnitude and direction of the combined suspension force and the x-axis and y-axis components remain constant at any moment, as shown in Fig. 1(a).

When the magnetic field angular frequency satisfies $\omega_m\neq\omega_n$, the x-axis and the y-axis component of the suspension force contain the time variable $(\omega_m-\omega_n)t$, resulting in the fluctuation of the combined suspension force with time, as shown in Fig. 1(b).

Combined with Fig. 1(a, b), the angular frequency of the magnetic field is the key factor affecting the magnitude

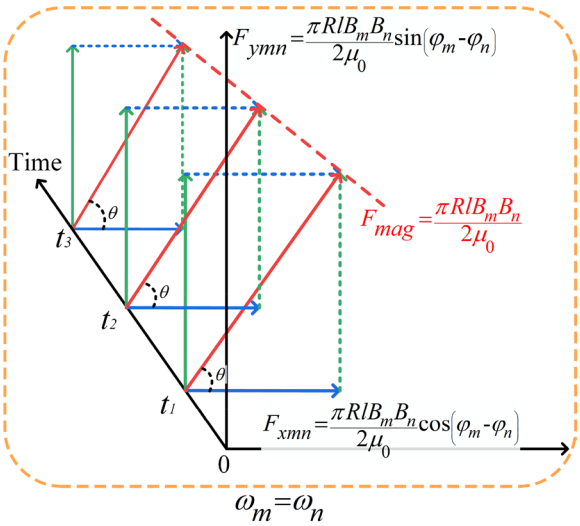

(a) Constant component of the suspension force

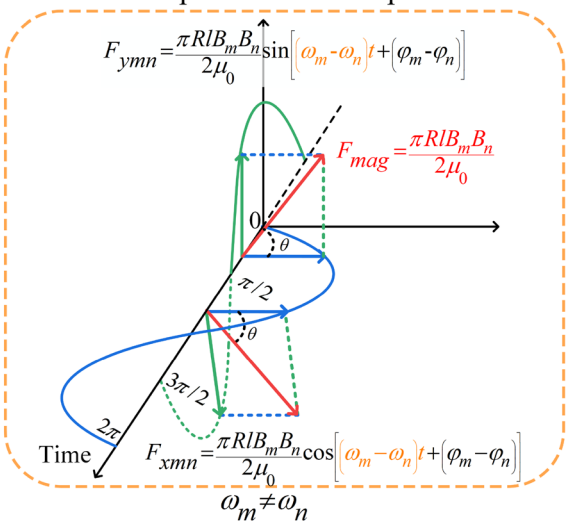

(b) Fluctuation component of the suspension force

Fig. 1 The suspension force vector diagram of BPMSM

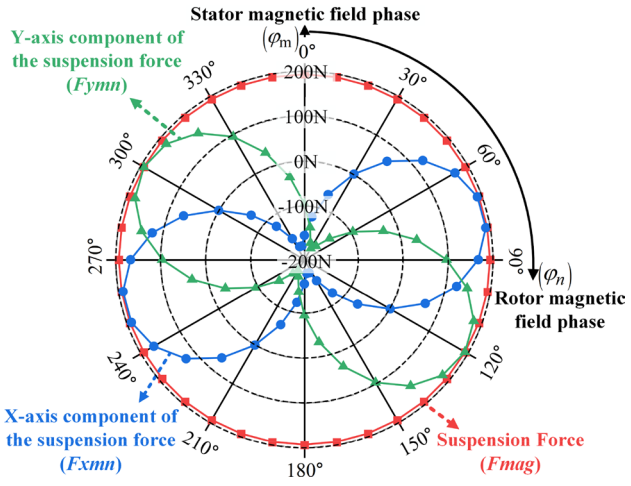

Fig. 2 The Relationship between magnetic field phase and radial suspension force of BPMSM

of the x-axis and y-axis suspension force components. The numerical relationship between the ω_m and ω_n determines the fluctuation of suspension force and its components.

Combined with the finite element analysis method, the influence of magnetic field phase on the magnitude and direction of suspension force is further investigated, as shown in Fig. 2. With the increase of the phase difference between the magnetic field of the permanent magnet and the magnetic field of the suspension winding ($\varphi_{m-}\varphi_n$), the magnitude of the x-axis component of the suspension force increases from 0 to 192N in the interval (30° ~ 120°) and the interval (210° ~ 300°) and then decreases to 0N in the interval (120° ~ 210°) and (300° ~ 30°) after changing from 0N to − 192 N. Similarly, the intervals where the magnitude of the y-axis component of the suspension force is greater than 0 are (75° ~ 165°) and (255° ~ 345°), and the intervals where the magnitude of the y-axis component of the suspension force is less than 0 are (345° ~ 75°) and (165° ~ 255°).

According to the finite element results, the variation of the x-axis and y-axis components of the suspension force affects the direction of the combined suspension force. When the magnetic field magnitudes B_m and B_n are constant, the magnitude of the combined suspension force is not affected by the change of the magnetic field phase angle (the suspension force is constant at 192N), which is consistent with the variation mechanism of (4).

In summary, the magnetic field angular frequency determines the fluctuation of the suspension force, and the magnetic field phase affects the direction of the suspension force of the BPMSM. The variation of the fluctuating component of the suspension force affects the stability of the operation of the BPMSM., while the variation of the magnitude of the x-axis and y-axis components of the suspension force determines the direction of the BPMSM in the radial two degrees of freedom.

3 The Multi-Harmonic Air Gap Magnetic Field Composition of the BPMSM

Due to the coupling effect among the magnetic field of the torque winding, the magnetic field of the suspension winding and the magnetic field of the permanent magnet, the variety of the multi-harmonic magnetic fields in the motor is increased, and the difficulty of the decoupling analysis of the suspension force is increased. Therefore, in order to obtain the influence of the multi-harmonic magnetic field on the magnitude, fluctuation and direction of the suspension force of the BPMSM, the analysis of the composition of the air gap magnetic field is an important part of the research.

Combined with the magnetomotive force and permeability analysis, the coupling magnetic field types of the magnetomotive force source and the permeability in the BPMSM are divided into the following four types: the main wave magnetic field interacted by the main wave magnetomotive force and the constant component of permeability, the permeability harmonic magnetic field interacted by the main wave magnetomotive force and the harmonic component of permeability, the magnetomotive force harmonic magnetic field interacted by the harmonic magnetomotive force and the constant component of permeability, and the magnetomotive force-permeability harmonic magnetic field interacted by the harmonic magnetomotive force and the harmonic component of permeability. as shown in Fig. 3

The air gap magnetomotive force is composed of the torque winding magnetomotive force (represented by the subscript d), the suspension winding magnetomotive force (represented by the subscript s), and the permanent magnet magnetomotive force (represented by the subscript m). Since the mathematical expressions of the torque winding magnetomotive force is similar to that of the suspension winding magnetomotive force, the expressions of the fundamental wave magnetomotive force and v-th harmonic magnetomotive force generated by the torque winding current are only given below [15].

Where, ω_{Vd} represents the v-th harmonic angular frequency, φ_d and φ_{Vd} represent the initial phase of the fundamental magnetomotive force and v-th harmonic magnetomotive force of the torque winding, respectively.

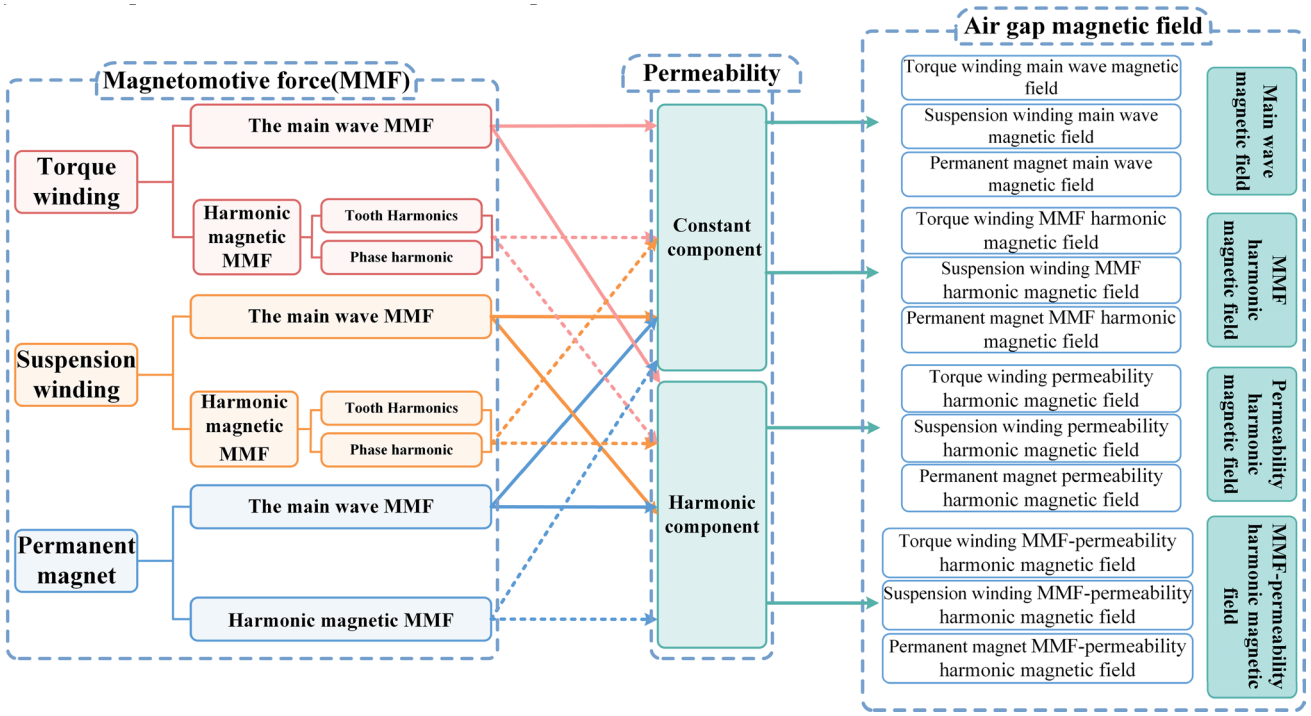

Fig. 3 The air gap magnetic field composition of BPMSM

$$\begin{cases} f_{pd}(\theta,t) = \dfrac{4}{\pi}\dfrac{\sqrt{2}N_d k_{Wd}}{2P_d} I_d \cos P_d\theta \cos\ \omega_d t \\ \quad = F_{Pd}\cos\left(P_d\theta - \omega_d t + \varphi_d\right) \\ f_{Vd}(\theta,t) = \dfrac{4}{\pi}\dfrac{\sqrt{2}N_d k_{Wvd}}{2V_d} I_d \cos v_d\theta \cos\omega_{Vd} t \\ \quad = F_{Vd}\cos\left(V_d\theta - \omega_{Vd} t + \varphi_{Vd}\right) \end{cases} \tag{7}$$

Affected by the distribution of the stator winding and the stator slotting, the winding harmonic magnetomotive force is divided into the phase band harmonic winding magnetomotive force and the tooth harmonic winding magnetomotive force, which are expressed by the V_{dx} and the V_{dc}, respectively.

$$\begin{cases} V_{dx} = (6k_{dx}+1)P_d\, k_{dx} = \pm1, \pm2, \pm3\cdots \\ V_{dc} = k_{dc}Z_1 + P_d\, k_{dc} = \pm1, \pm2, \pm3\cdots \end{cases} \tag{8}$$

And the mathematical expressions for the main wave magnetomotive force and harmonic magnetomotive force generated by the permanent magnet excitation source are shown in (9) [14].

$$\begin{cases} f_\alpha(\theta,t) = F_\alpha\cos\left(P_\alpha\theta - \omega_\alpha t + \varphi_\alpha\right) \\ f_\mu(\theta,t) = \sum F_\mu\cos\left(P_\mu\theta - \omega_\mu t + \varphi_\mu\right) \end{cases} \tag{9}$$

where, $\omega_\mu = \mu\omega_\alpha$, $P_\mu = (2k_\mu + 1)P_\alpha$, $k_\mu = 1, 2, 3\cdots$.

Due to the surface mounted structure of the BPMSM, it is only necessary to consider the variation of the air gap permeability caused by the stator slotting. Therefore, the air gap permeability distributed along the circumference can be expressed as.

$$\Lambda(\theta,\gamma) = \Lambda_0 + \sum\Lambda_h = \Lambda_0 + \sum\Lambda_\beta\cos\left(\beta Z_1\theta + \gamma\right) \tag{10}$$

$$
\begin{aligned}
b(\theta,t) =& f(\theta,t)\Lambda(\theta,\gamma)\\
=& f_{Pd}(\theta,t)\Lambda_0 + f_{Ps}(\theta,t)\Lambda_0 + f_{P\alpha}(\theta,t)\Lambda_0 + \sum f_{Vd}(\theta,t)\Lambda_0 + \sum f_{Vs}(\theta,t)\Lambda_0 + \sum f_{\mu}(\theta,t)\Lambda_0\\
&+ \sum f_{Pd}(\theta,t)\Lambda_h + \sum f_{Ps}(\theta,t)\Lambda_h + \sum f_{P\alpha}(\theta,t)\Lambda_h + \sum f_{Vd}(\theta,t)\sum \Lambda_h + \sum f_{Vs}(\theta,t)\sum \Lambda_h + \sum f_{\mu}(\theta,t)\sum \Lambda_h\\
=& F_{Pd}\Lambda_0 \cos\left(P_d\theta - \omega_d t + \varphi_d\right) + F_{Ps}\Lambda_0 \cos\left(P_s\theta - \omega_s t + \varphi_s\right) + F_{P\alpha}\Lambda_0 \cos\left(P_\alpha\theta - \omega_\alpha t + \varphi_\alpha\right)\\
&+ \sum F_{Vd}\Lambda_0 \cos\left(V_d\theta - \omega_{Vd} t + \varphi_{Vd}\right) + \sum F_{Vs}\Lambda_0 \cos\left(V_s\theta - \omega_{Vs} t + \varphi_{Vs}\right) + \sum F_{\mu}\Lambda_0 \cos\left(P_\mu\theta - \omega_\mu t + \varphi_\mu\right)\\
&+ \sum F_{Pod} \cos\left(P_{od}\theta - \omega_{od} t + \varphi_{od}\right) \sum \Lambda_\beta \cos\left(\beta Z_1\theta + \gamma\right) + \sum F_{Pos} \cos\left(P_{os}\theta - \omega_{os} t + \varphi_{os}\right) \sum \Lambda_\beta \cos\left(\beta Z_1\theta + \gamma\right)\\
&+ \sum F_{Po\alpha} \cos\left(P_{o\alpha}\theta - \omega_{o\alpha} t + \varphi_{o\alpha}\right) \sum \Lambda_\beta \cos\left(\beta Z_1\theta + \gamma\right)\\
&+ \sum F_{Vod} \cos\left(V_{od}\theta - \omega_{Vod} t + \varphi_{Vod}\right) \sum \Lambda_\beta \cos\left(\beta Z_1\theta + \gamma\right) + \sum F_{Vos} \cos\left(V_s\theta - \omega_{Vos} t + \varphi_{Vos}\right) \sum \Lambda_\beta \cos\left(\beta Z_1\theta + \gamma\right)\\
&+ \sum F_{o\mu} \cos\left(P_{o\mu}\theta - \omega_{o\mu} t + \varphi_{o\mu}\right) \sum \Lambda_\beta \cos\left(\beta Z_1\theta + \gamma\right)
\end{aligned}
\tag{11}
$$

where, Z_1 is the number of stator slots, Λ_0 is the constant component of magnetic conductivity, Λ_h is the harmonic component of magnetic conductivity, and γ is the relative position between the stator and rotor.

Therefore, the mathematical expression of the air gap magnetic field of the BPMSM is shown in (11).

Due to the different coupling of the magnetomotive force and air gap magnetic permeability, the air gap of BPMSM contained 12 types of magnetic fields. And according to the difference of the magnitude of the air gap magnetic field, it is divided into four categories, such as the main wave magnetic field, the magnetomotive force harmonic magnetic field, the air gap permeability harmonic magnetic field and the magnetomotive force-permeability harmonic magnetic field.

Among them, the main wave magnetic field and the magnetomotive force harmonic magnetic field have the large magnetic field magnitude and the low harmonic order. And the air gap permeability harmonic magnetic field and the magnetomotive force-permeability harmonic magnetic field has the small magnetic field magnitude and high harmonic order.

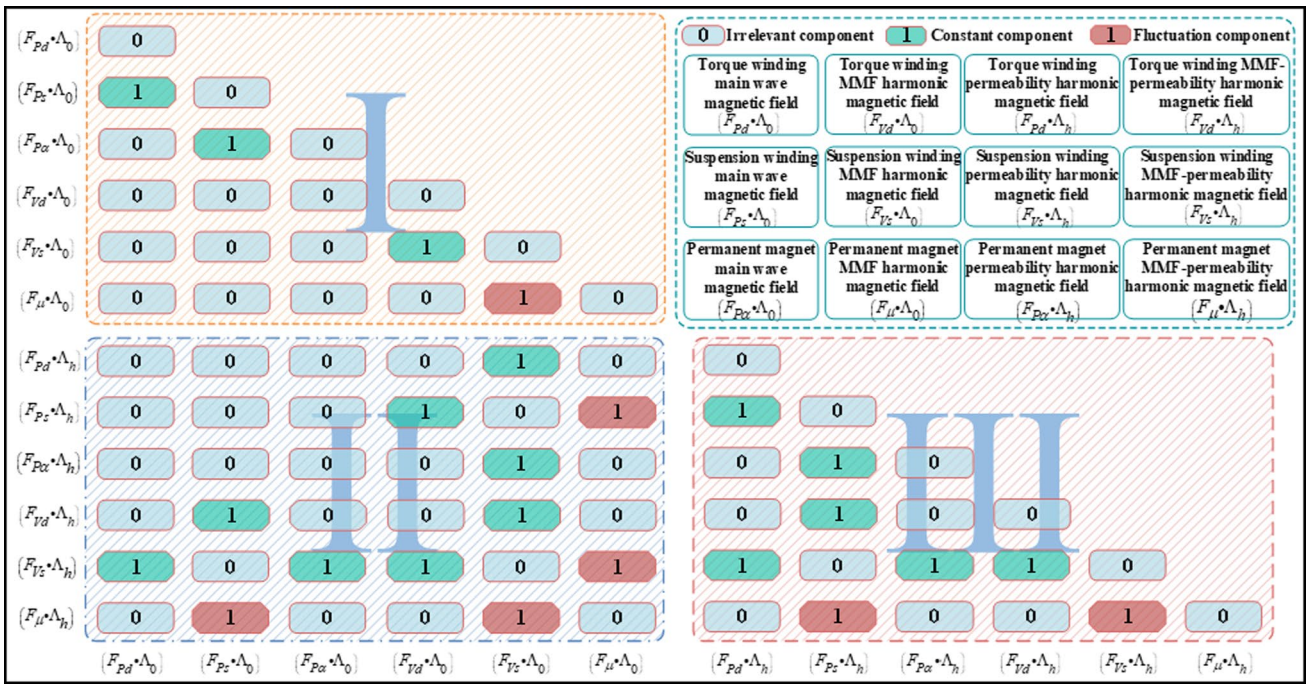

Fig. 4 The relationship between the multi-harmonic magnetic field and the radial electromagnetic force of BPMSM

Under the influence of coupling magnetic field, there is a large number of electromagnetic force waves in the motor, which causes the vibration noise of the motor is increased, and the suspension stability of the BPMSM is also affected. Therefore, on the basis of the characteristics of the air gap magnetic field distribution of the BPMSM and the Maxwell stress tensor method, the correspondence between the coupling magnetic field and the radial suspension force is further investigated in this paper.

4 Research on the Suspension Characteristics Under the Multi-harmonic Magnetic Field Coupling

4.1 Analysis of the Main Constituent of the Radial Suspension Force of BPMSM

In the part I of the Fig. 4, the radial electromagnetic force is generated by the interaction of the magnetic field constituted by the magnetomotive force and the constant component of the magnetic permeability, and it contains the following six forms of the magnetic field ($F_{Pd}\Lambda_0$、$F_{Ps}\Lambda_0$、$F_{P\alpha}\Lambda_0$、$F_{\mu}\Lambda_0$、$F_{Vd}\Lambda_0$、$F_{Vs}\Lambda_0$). Because the magnetic field in this part has the characteristics of large magnitude and low frequency order, the constant component magnitude of the suspension force is the key for the suspension operation of the BPMSM., and the magnitude of the fluctuation component of the suspension force affects the vibration noise and suspension stability of the motor operation.

$$\begin{aligned} F_{Pvs\mu x} =& \frac{Rl}{2\mu_0}\int_0^{2\pi}\frac{B_{Pvs}^2}{4}\cos\left[\left(2P_{vs}\pm 1\right)\theta - 2\omega_{vs}t + 2\varphi_{vs}\right] + \frac{B_{Pvs}^2}{2}\cos\theta + \frac{B_{\mu}^2}{4}\cos\left[\left(2P_{\mu}\pm 1\right)\theta - 2\omega_{\mu}t + 2\varphi_{\mu}\right] \\ &+\frac{B_{\mu}^2}{2}\cos\theta + \frac{B_{Pvs}B_{\mu}}{2}\cos\left[\left(P_{vs}\pm P_{\mu}\pm 1\right)\theta - \left(\omega_{vs}\pm\omega_{\mu}\right)t + \left(\varphi_{vs}\pm\varphi_{\mu}\right)\right]d\theta \\ &\xrightarrow[P_{vs}\pm P_{\mu}\pm 1]{}\frac{\pi RlB_{Pvs}B_{\mu}}{2\mu_0}\cos\left[\varphi_{vs}-\varphi_{\mu}-\left(\omega_{vs}-\omega_{\mu}\right)t\right] \end{aligned} \tag{12}$$

The radial electromagnetic force in the BPMSM can be divided into the constant component of the suspension force and the fluctuation component of the suspension force. The constant component of the suspension force determines the magnitude of the force that is generated by the steady operation of the motor, while the fluctuation component of the suspension force affects the vibration and noise during the operation of the motor.

Therefore, in this paper, based on the mathematical analysis model of the suspension force and the analysis of the air gap multi-harmonic magnetic field, the influence of the coupling magnetic field on the radial suspension force is further analyzed by combining the expression of suspension force, and the classification research is done with the different influence of the magnetic field on the suspension force, as shown in Fig. 4. The number 1 indicates that the radial electromagnetic force is related to the suspension performance of the BPMSM, while the number 0 indicates that the radial electromagnetic force is irrelevant to the suspension performance of the BPMSM. The color is used to distinguish the effect of radial electromagnetic force, the green color corresponds to the constant component of the suspension force and the red color corresponds to the fluctuation component of the suspension force.

Among them, the fluctuation component of the radial electromagnetic force generated by the interaction of the harmonic magnetic field of the magnetomotive force of the permanent magnet ($F_{\mu}\Lambda_0$) and the harmonic magnetic field of the suspension winding magnetomotive force ($F_{Vs}\Lambda_0$), as shown in (12), and corresponding to the red-colored square 1 of the Fig. 4.

The constant component of the suspension force resulting from the interaction of the main wave magnetic field of the torque winding ($F_{Pd}\Lambda_0$) with the main wave magnetic field of the suspension winding ($F_{Ps}\Lambda_0$), as shown in (13), and corresponding to the green-colored square 1 of the Fig. 4.

$$\begin{aligned} F_{Pd\,Ps\,x} =& \frac{Rl}{2\mu_0}\int_0^{2\pi}\frac{B_{Pd}B_{Ps}}{2}\cos\left[\left(P_d\pm P_s\pm 1\right)\theta - \left(\omega_d\pm\omega_s\right)t + \left(\varphi_d\pm\varphi_s\right)\right]d\theta \\ =& \frac{\pi RlB_{Pd}B_{Ps}}{2\mu_0}\cos\left(\varphi_d-\varphi_s\right) \end{aligned} \tag{13}$$

By comparing (12) and (13), due to the different angular frequency of the coupling magnetic field ($\omega_{vs}\neq\omega_{\mu}$), it leads to the time variable of the suspension force, which results in the fluctuation component of the suspension force (12). And the fluctuation period of the suspension force is influenced by the angular frequency difference of the coupling magnetic field.

Combined with the correspondence between the multi-harmonic magnetic field and the radial suspension force

shown in Fig. 4, and the expression of the suspension force component, the characteristic parameters of the coupling magnetic field (such as magnetic field size, magnetic field phase and magnetic field angular frequency, etc.) can be transformed to quickly obtain the rest of the expression for the suspension force of the BPMSM.

4.2 Analysis of the Secondary Constituent of the Radial Suspension Force of BPMSM

The radial suspension force in the part II of the Fig. 4 is generated by the action of the magnetomotive force with the constant component of the magnetic permeability and the harmonic component of the magnetic permeability. Since there are more types of the coupling air gap magnetic fields (including four major types of magnetic fields such as the main wave magnetic field, magnetomotive force harmonic magnetic field, permeability harmonic magnetic field and magnetomotive force-permeability harmonic magnetic field), when the magnetic fields interact with each other, more forms of the radial suspension force are generated. However, according to the characteristic of the coupling magnetic field, the radial suspension force of this part has the characteristics of small magnitude and short fluctuation period, which is the secondary composition of radial suspension force of BPMSM.

$$
\begin{aligned}
F_{Pos\mu x} = {} & \frac{Rl}{2\mu_0}\int_0^{2\pi}\frac{B_{Pos}^2}{16}\cos\left[\left(2P_{os}\pm 2\beta Z_1\pm 1\right)\theta-2\omega_s t+2\varphi_s\pm 2\gamma\right)\right]+\\
& \frac{B_\mu^2}{4}\cos\left[\left(2P_\mu\pm 2\beta Z_1\pm 1\right)\theta-2\omega_\mu t+2\varphi_\mu\pm 2\gamma\right)\right]\\
& +\frac{B_\mu^2}{2}\cos\theta+\frac{B_{Pos}^2}{8}\cos\theta+\frac{B_{Pos}B_\mu}{4}\cos\left[\left(P_{os}\pm P_\mu\pm\beta Z_1\pm 1\right)\right.\\
& \left.\theta-\left(\omega_{Pos}\pm\omega_\mu\right)t+\left(\varphi_{Pos}\pm\varphi_\mu\pm\gamma\right)\right]d\theta\xrightarrow[\omega_s\neq\omega_\mu]{}\frac{\pi RlB_{Pos}B_\mu}{4\mu_0}\\
& \cos\left[\left(\varphi_{Pos}\pm\varphi_\mu\pm\gamma\right)-\left(\omega_{Pos}\pm\omega_\mu\right)t\right]
\end{aligned}
\tag{14}
$$

$$
\begin{aligned}
F_{Posoo\mu x} = {} & \frac{Rl}{2\mu_0}\int_0^{2\pi}\frac{B_{Pos}^2}{16}\cos\left[\left(2P_{os}\pm 2\beta Z_1\pm 1\right)\theta-2\omega_s t+2\varphi_{os}\pm 2\gamma\right]\\
& +\frac{B_{o\mu}^2}{16}\cos\left[\left(2P_{o\mu}\pm 2\beta Z_1\pm 1\right)\theta-2\omega_\mu t+2\varphi_{o\mu}\pm 2\gamma\right]+\frac{B_{o\mu}^2}{8}\cos\theta\\
& +\frac{B_{Pos}^2}{8}\cos\theta+\frac{B_{Pos}B_\mu}{8}\cos\left[\left(\left(P_{os}\pm\beta Z_1\right)\pm\left(P_\mu\pm\beta Z_1\right)\pm 1\right)\theta\right.\\
& \left.-\left(\omega_s\pm\omega_\mu\right)t+\left(\varphi_{os}\pm\gamma\right)\pm\left(\varphi_\mu\pm\gamma\right)\right]d\theta\\
= {} & \begin{cases}\xrightarrow[P_{os}\pm\beta Z_1+P_\mu\pm\beta Z_1\pm 1=0]{}\dfrac{\pi RlB_{Pos}B_\mu}{8\mu_0}\cos\left[\varphi_{os}+\varphi_\mu\pm 2\gamma-\left(\omega_s+\omega_\mu\right)t\right]\\ \xrightarrow[P_{os}-P_\mu\pm 1=0]{}\dfrac{\pi RlB_{Pos}B_\mu}{8\mu_0}\cos\left[\varphi_{os}-\varphi_\mu-\left(\omega_s-\omega_\mu\right)t\right]\end{cases}
\end{aligned}
\tag{15}
$$

The expression of the fluctuation component of the radial electromagnetic force is generated by the interaction of the suspension winding magnetomotive force-permeability harmonic magnetic field ($F_{Ps}\Lambda_h$) and the permanent magnet magnetomotive force harmonic magnetic field ($F_\mu\Lambda_0$), as shown in (14).

Compared to the expression for the fluctuating component of the suspension force (12), the factor affecting the fluctuating component of the suspension force (14) has added the relative position (γ) between the stator and the rotor, also the magnitude of the expression coefficients is reduced by 50%. Meanwhile, due to the influence of the harmonic component of the air gap permeability (Λ_h), the fluctuation frequency of fluctuation component of the suspension force increases, leading to a decrease in the smoothness of the suspension force waveform.

4.3 Analysis of the Micro Constituent of the Radial Suspension Force of BPMSM

In the part III of the Fig. 4, the radial electromagnetic force is generated by the interaction of the magnetic field which is composed of the magnetomotive force and the air gap permeability harmonics, and it contains the following six

Table 1 The key parameters of the prototype

Parameters (unit)	Value	Parameters (unit)	Value
Rated power (kW)	8.5	Number of stator slots	36
Torque current(A)	18.6	Suspension current (A)	4
Turn number of torque winding	24	Turn number of suspension winding	22
Number of pole pairs of torque winding	2	Number of pole pairs of suspension winding	1
Stator outer diameter (mm)	180	Rotor outer diameter (mm)	96.4
Stator inner diameter (mm)	103	Iron core axial length (mm)	72

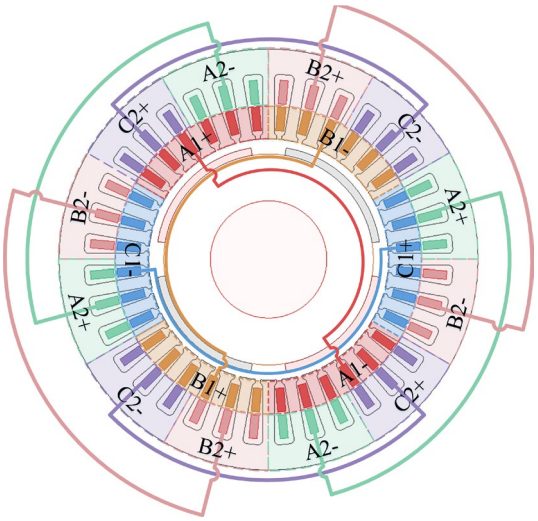

Fig. 5 The stator dual windings arrangement of BPMSM

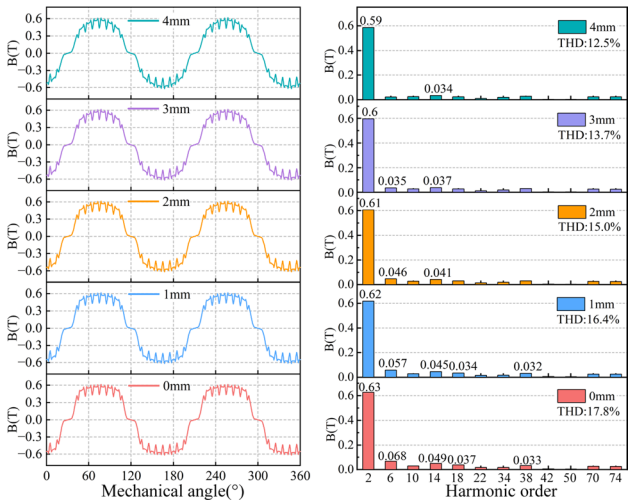

Fig. 6 The variation of the harmonic content of the no-load air gap magnetic field with different eccentric distances

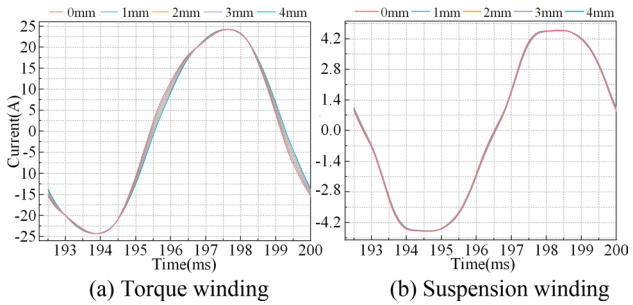

Fig. 7 The waveform of current

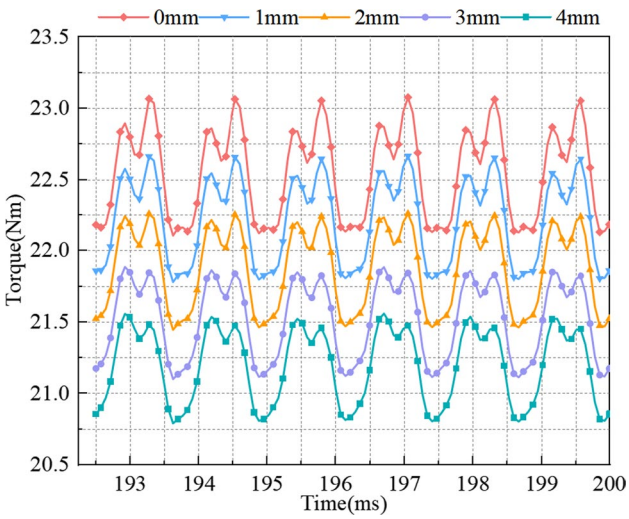

Fig. 8 The waveform of torque

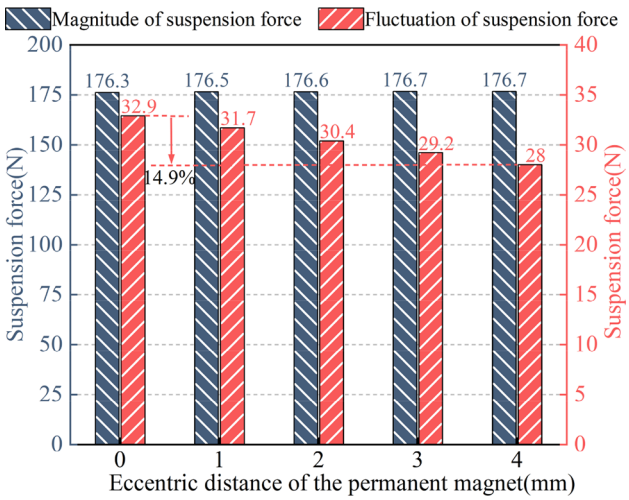

Fig. 9 The relationship between the eccentric distance of the permanent magnet and the suspension force

magnetic field forms ($F_{Pd}\Lambda_h$、$F_{Ps}\Lambda_h$、$F_{P\alpha}\Lambda_h$、$F_{\mu}\Lambda_h$、$F_{Vd}\Lambda_h$、$F_{Vs}\Lambda_h$). Moreover, the coupling magnetic field in this part has the characteristics of the high harmonic order and the small magnitude.

The expression of the suspension force generated by the interaction of the suspension winding magnetomotive force-permeability harmonic magnetic field ($F_{Ps}\Lambda_h$) and the permanent magnet magnetomotive force-permeability harmonic magnetic field ($F_{\mu}\Lambda_h$) is given in (15). Due to the different parameters of the coupling magnetic field, the different expressions for the fluctuation components of the suspension force ($F_{Posoμx}$) are obtained.

Due to the different of the magnetic field pole pairs and the harmonic orders, under the same coupling magnetic field, the magnitude and the fluctuation period of the

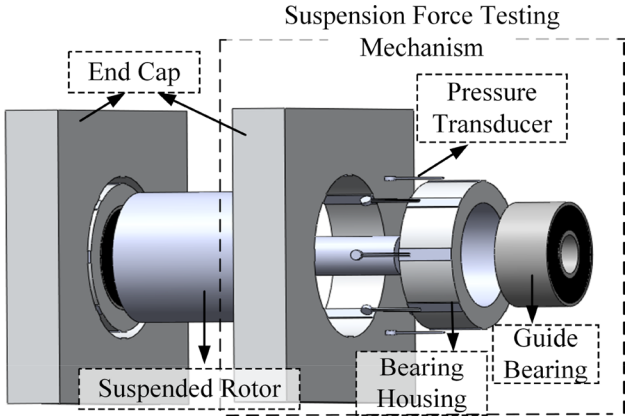

Fig. 10 The measurement diagram of suspension force

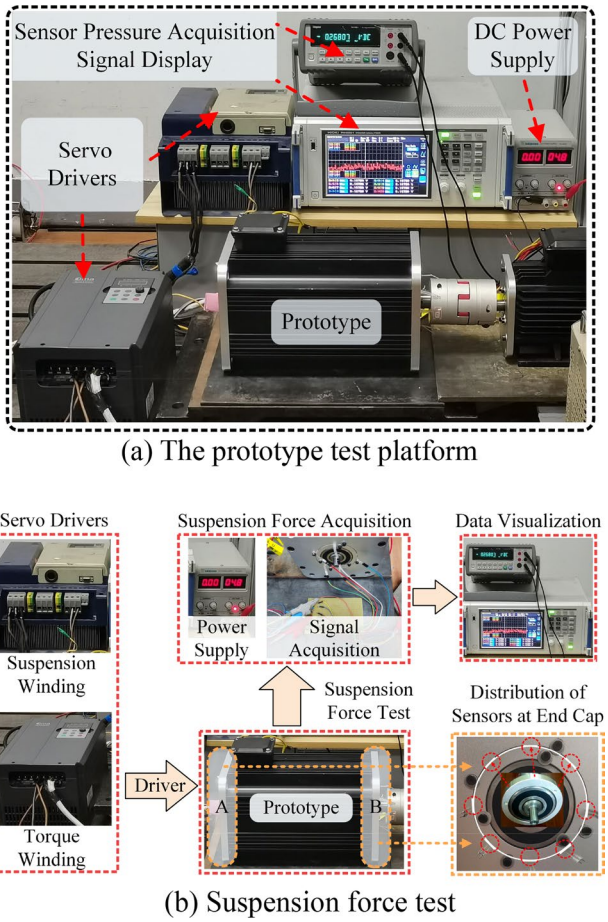

Fig. 11 Suspension force test of the prototype

suspension force component are affected by the different magnetic field phase ($\varphi_{os} + \varphi_{\mu} \pm 2\gamma$ and $\varphi_{os} - \varphi_{\mu}$) and magnetic field angular frequency ($\omega_s + \omega_{\mu}$ and $\omega_s - \omega_{\mu}$) of the fluctuation component of the suspension force, so that the expression of the radial electromagnetic force as shown in (14) is obtained.

In addition, compared with the (12) of the fluctuating component of the suspension force in the first part, the coefficient of the expression of the suspension force in this part is changed from 1/2 to 1/8, which is reduced by 75%. Moreover, the magnitude of the magnetic fields is small, and the harmonic orders are high, thus the magnitude of the fluctuation component of the suspension force and the constant component of the suspension force are small and negligible.

5 Verification of the BPMSM by Finite Element Analysis and Prototype Test

In this paper, the composition of the multi-harmonic magnetic field of the bearingless permanent magnet synchronous motor is analyzed, and the mathematical expressions of the multi-harmonic magnetic field and the suspension force of the motor are obtained, and the important factors that affect the magnitude and fluctuation of the suspension force are determined.

In order to verify the correctness of the analysis, the mechanism of the suspension force of the bearingless permanent magnet synchronous motor is further investigated in this paper by using the finite element method, the numerical analysis method and the experimental test. The key parameters of the prototype are given in Table 1, the stator dual windings arrangement relationship are given in the Fig. 5, where A1, B1 and C1 are the suspension windings, and A2, B2 and C2 are the torque windings.

Based on the above analysis, the harmonic magnetic field of the permanent magnet is the main factor that causes the fluctuation of the suspension force. In order to determine the relationship between the harmonic magnetic field of the permanent magnet and the fluctuation of the suspension force, the finite element method is firstly used to investigate the harmonic content of the no-load air gap magnetic field of with different eccentric distances, as shown in Fig. 6.

The amplitude of suspension force and suspension fluctuation during a stable cycle are analyzed. The current for this stable cycle is shown in Fig. 7. The torque waveform of this stable cycle is shown in Fig. 8.

The variation of the magnitude and the fluctuation of the suspension force is given in Fig. 9. With the increase of the polar arc eccentricity of the permanent magnet, the magnitude of the radial suspension force remains basically the same, while the fluctuation of the radial suspension force gradually decreases. When the pole arc eccentricity of permanent magnet is 0 mm, the magnitude of radial suspension force and its fluctuation are 176.3N and 32.9N respectively, while when the pole arc eccentricity of permanent magnet increases to 4 mm, the magnitude of radial suspension force

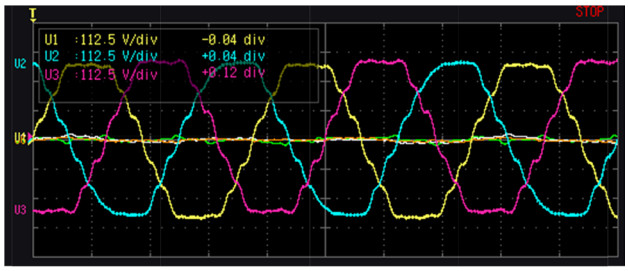

(a) The prototype tests

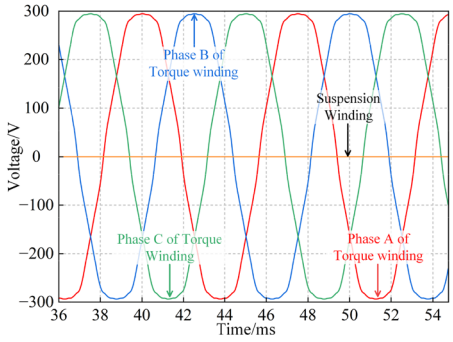

(b)The finite element calculation results

Fig. 12 The back electromotive force comparison **a** the prototype tests **b** The finite element calculation results

Table 2 The suspension force comparison of the static test and finite element calculation with different current

Current (A)	Test results (N)	FEM results (N)	Relative error (N)
1.5	21.0	22.1	1.1
2.0	28.2	29.5	1.3
2.5	35.2	37.51	2.3
3.0	41.6	45.5	3.9
3.5	50.9	53.7	2.8

Table 3 The test conditions of dynamic suspension test

Parameters(unit)	Value	Parameters(unit)	Value
The V/f of the suspension winding	1.65	The voltage of the suspension winding(V)	0.8
Eccentric distances(mm)	0	Torque of load (Nm)	0

and its fluctuation are 176.7N and 28N. By comparison, the magnitude of radial suspension force increases by 0.2%, while the fluctuation of radial suspension force decreases by 14.9%.

Based on the above analysis, the experimental prototype is tested to verify the correctness of the theoretical analysis.

Table 4 The suspension force comparison of the dynamic test, FEM and analytical calculation with different frequencies

Frequency (Hz)	Test results (N)	FEM results (N)	Analytical calculation results (N)
20	26.2	28.4 ± 1.6	31.1
30	28.4	27.6 ± 2.1	31.3
40	28.3	27.7 ± 2.0	31.5
50	27.7	28.4 ± 2.5	31.7

As shown in Fig. 10, the suspension force measurement sensors are placed at the end cap. The pressure sensors that are used to measure the radial suspension force are placed between the specially manufactured bearing chamber and the end cap. The eight pressure sensors are placed around the bearing chamber.

The prototype is tested on the experimental platform as shown in Fig. 11. The experimental equipment includes the servo drives, prototype, power analyzer, and the voltage signal acquisition circuit.

Figure 11(a) shows the suspension force test platform of the prototype, and Fig. 11(b) shows the suspension force test. When the prototype is operated, the pressure signal is collected through the sensors at the end caps of the motor and the signal acquisition circuit. The collected signals are displayed by the oscilloscope.

(1) The No-load Back Electromotive Force Tests: the prototype test curve and the finite element calculation result are given in Fig. 12. The finite element calculation results are consistent with the prototype tests, and the difference between the RMS of the back electromotive force of the prototype test and finite element calculation results is only 0.3%. And the THD of the back electromotive force of test is 6.14%. The THD of the back electromotive force of finite element calculation is 6.53%. The finite element calculation results are consistent with the prototype tests, and the difference between the test and finite element calculation results is only 4.5%.

(2) The Static Suspension Test: To study the variation of the suspension force with the suspension winding current, the suspension test is performed on the prototype at 0 rpm. With the increase of the suspension current, the data of each sensor are recorded, and then the measured suspension force is obtained. Thefinite element calculation results are also given in Table 2.

Comparing the results of experiments and finite element calculation, the suspension force gradually increases with the increase of suspension current. When the suspension current changes from 1.5A to 3.5A, the magnitude of suspension force of the proto-

type test changes from 21.0N to 50.9N, and the magnitude of suspension force of the finite element calculation results changes from 22.1N to 53.7N. The results of the prototype tests are consistent with the results of the finite element calculation results. The maximum relative error is 3.9N (8.6%).

(3) The Dynamic Suspension Test: To study the dynamic suspension characteristics of the prototype, the radial suspension force of the prototype is measured at different frequencies, and the test conditions are shown in Table 3. The test results of the radial suspension force are shown in Table 4. Also, the finite element calculation results and analytical calculation results at different frequencies are also given in the Table 4.

As can be seen from Table 4, with the increase of frequency, the magnitude of the suspension force remains constant. When the frequency of the motor is changed from 20 to 50 Hz, the finite element calculation results are around 28N, the analytical calculation results and prototype test are around 31.4N and 27.3N, respectively. The maximum relative error of the radial force between the finite element calculation and the prototype test is 2.2N (7.9%). And the maximum relative error between the finite element calculation results and the analytical calculation results is 3.8N (13.6%).

6 Conclusions

In this paper, the problem of radial suspension force fluctuation in the motor design optimization process is investigated. An analysis method is proposed to quickly determine the key factors that affect the suspension performance of the BPMSM, which can target the magnetic field that causes the variation of the suspension force so as to carry out the accurate optimization.

The analysis results show that the harmonic magnetic field of the permanent magnet is the key factor that causes the fluctuation of the suspension force. When the pole arc eccentric distance of the permanent magnet is changed from 0 to 4 mm, the total harmonic distortion rate is reduced by 33.9%, the fluctuation of the suspension force is reduced by 16.6%, and the suspension force magnitude is changed by only 0.3%.

Acknowledgements This work was supported in part by the National Natural Science Foundation of China under Grant U2004183, 52177063. And in part by Excellent Young Scholars Project of Henan Province under Grant 232300421070, and in part by the University Science and Technology Innovation Talent Support Program of Henan province under Grant 23HASTIT026, and in part by the Henan Province Science and Technology Research Program under Grant 232102220080.

References

1. Pei T, Li D, Liu J, Li J, Kong W (2022) Review of bearingless synchronous motors: principle and topology. IEEE Transact Transport Electrif 8(3):3489–3502. https://doi.org/10.1109/TTE.2022.3164420
2. Fu Y, Takemoto M, Ogasawara S, Orikawa K (2020) Investigation of operational characteristics and efficiency enhancement of an ultrahigh-speed bearingless motor at 100 000 r/min. IEEE Transact Industry Appl 56(4):3571–3583. https://doi.org/10.1109/TIA.2020.2986453
3. Matsuzaki T, Takemoto M, Ogasawara S, Ota S, Oi K, Matsuhashi D (2017) Operational characteristics of an IPM-type bearingless motor with 2-pole motor windings and 4-pole suspension windings. IEEE Transact Industry Appl 53(6):5383–5392. https://doi.org/10.1109/TIA.2017.2746668
4. Yang Y, Liu J, Wang R, Wang H (2022) Complementarity analysis of consequent-pole bearingless flux reversal motor windings with different pitch matchings. AIP Adv 12(10):105207. https://doi.org/10.1063/5.0112054
5. Chen J, Zhu J, Severson EL (2020) Review of bearingless motor technology for significant power applications. IEEE Transact Industry Appl 56(2):1377–1388. https://doi.org/10.1109/TIA.2019.2963381
6. Kurita N, Ishikawa T, Saito N, Masuzawa T, Timms DL (2019) A dual-sided stator type axial bearingless motor development for total artificial heart. IEEE Transact Industry Appl 55(2):1516–1523. https://doi.org/10.1109/TIA.2018.2884609
7. Zhang T, Ye X, Mo L, Lu Q (2019) Electromagnetic performance analysis on the bearingless permanent magnet synchronous motor with Halbach magnetized rotor. IEEE Access 7:121265–121274. https://doi.org/10.1109/ACCESS.2019.2937897
8. Weinreb BS, Noh M, Fyler DC, Trumper DL (2021) Design and implementation of a novel interior permanent magnet bearingless slice motor. IEEE Transact Industry Appl 57(6):6774–6782. https://doi.org/10.1109/TIA.2021.3080663
9. Amemiya J, Chiba A, Dorrell DG, Fukao T (2005) Basic characteristics of a consequent-pole-type bearingless motor. IEEE Trans Magn 41(1):82–89. https://doi.org/10.1109/TMAG.2004.840179
10. Chiba A, Sotome K, Iiyama Y, Rahman MA (2011) A novel middle-point-current-injection-type bearingless PM synchronous motor for vibration suppression. IEEE Transact Industry Appl 47(4):1700–1706. https://doi.org/10.1109/TIA.2011.2155611
11. Zhu Z, Wang J, Cheng M (2021) A novel axial split phase bearingless flywheel machine with hybrid-inner-stator permanent magnet-based structure. IEEE Trans Energy Convers 36(3):1873–1882. https://doi.org/10.1109/TEC.2020.3045143
12. Pan W, Zhu H, Li H (2016) Design and optimization of bearingless permanent magnetic synchronous motors. IEEE Transact Appl Superconduct 26(4):5200704. https://doi.org/10.1109/TASC.2016.2516908
13. Wang H, Lu Y, Wu S, Guo L (2022) Optimization design of unequal amplitude modulated poles for the bearingless PMSM. Energies 15:3097. https://doi.org/10.3390/en15093097
14. Sun X et al (2016) Suspension force modeling for a bearingless permanent magnet synchronous motor using maxwell stress tensor method. IEEE Transact Appl Superconduct 26(7):1–5. https://doi.org/10.1109/TASC.2016.2599708
15. Liu F, Wang X, Xing Z, Yu A, Li C (2021) Reduction of cogging torque and electromagnetic vibration based on different combination of pole arc coefficient for interior permanent magnet synchronous machine. CES Transact Electr Mach Syst 5(4):291–300. https://doi.org/10.30941/CESTEMS.2021.00034
16. Fengxiang W, Longya X, (2000) Calculation and measurement of radial and axial forces for a bearingless PMDC motor.

In: Conference Record of the 2000 IEEE Industry Applications Conference. Thirty-Fifth IAS Annual Meeting and World Conference on Industrial Applications of Electrical Energy (Cat. No.00CH37129), Rome, Italy, 1: 249–252 https://doi.org/10.1109/IAS.2000.881105.

Hongbo Qiu received the M.S. degree in electrical engineering from the Harbin University of Science and Technology, Harbin, China, in 2012, and the Ph.D. degree in electrical engineering from the Harbin University of Science and Technology, in 2014. Since 2014, he has been with the Zhengzhou University of Light Industry, Zhengzhou, China. His research interests include electromagnetic and thermal analysis on electrical machines, especially in permanent magnetic machines.

Si Chen is working toward the M.S. degree in electrical machines at Zhengzhou University of Light Industry. His current research interests include electromagnetic, vibration, fault diagnosis and modal analysis of electric machines, especially high-voltage line-starting permanent magnet motor.

Guangchuan Liang received the M.S. degree in electrical engineering from Zhengzhou University of Light Industry, China, in 2023.He is working on his Ph.D. degree at Nanjing University of Aeronautics and Astronautics. His research interests include electromagnetic and thermal analysis of electric machines, especially high-speed permanent magnet motors.

Cunxiang Yang received the Ph.D. degree in electrical engineering from the Southeast University, in 1996. And He has been with the Zhengzhou University of Light Industry, Zhengzhou, China, since 1996. His research interests include electromagnetic and thermal analysis on electrical machine, especially in permanent magnetic machines.